Article
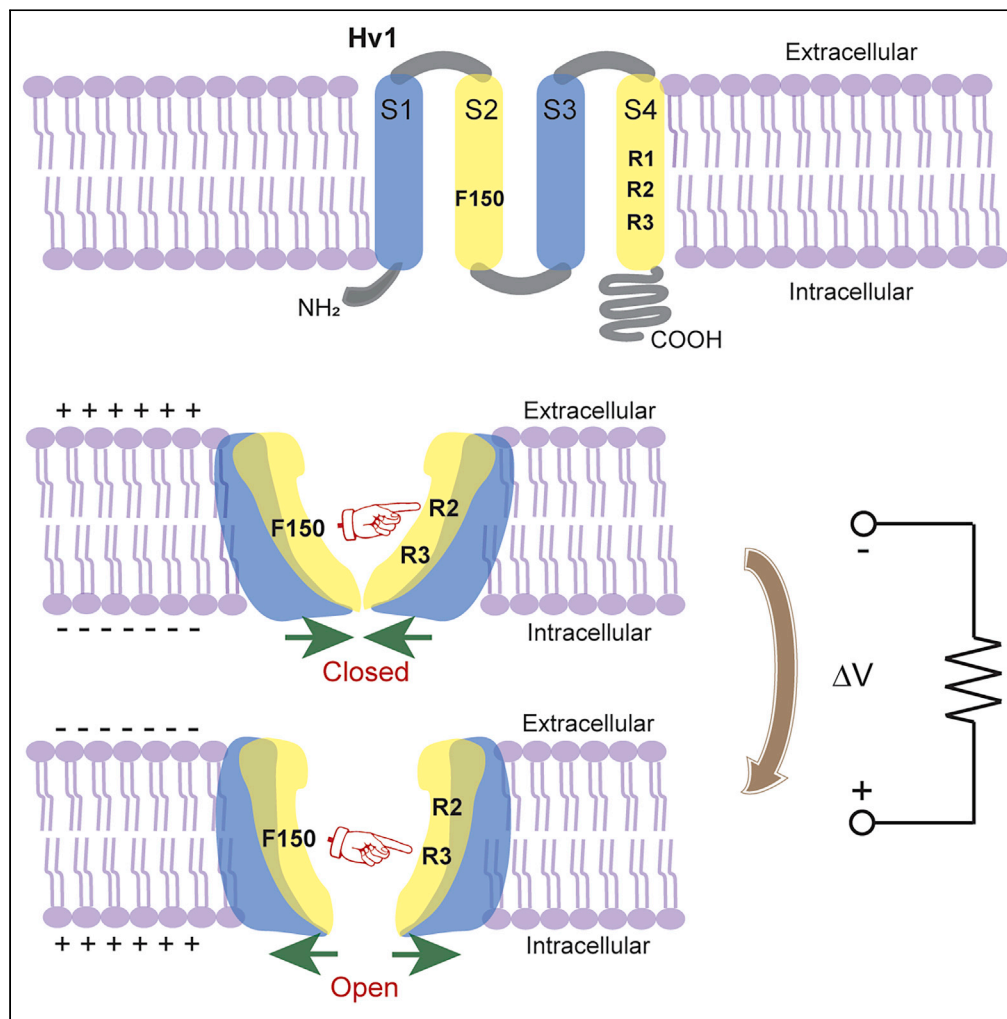
The role of Phe150 in human voltage-gated proton channel

Xin Wu, Lu Zhang, Liang Hong

hong2004@uic.edu

Highlights

Hydrophobicity of F150 is crucial for human H$_v$1 channel voltage-dependent activation

F150 interacts with R2 to stabilize the closed state of the H$_v$1 channel

When depolarized, R3 moves upward to interact with F150 stabilizing the open state of H$_v$1

F150 is essential for the transfer of the H$_v$1 arginines in the process of voltage sensing

Article

The role of Phe150 in human voltage-gated proton channel

Xin Wu,[1] Lu Zhang,[1] and Liang Hong[1,2,3,]*

SUMMARY

The voltage-gated proton channel H_v1 is a member of voltage-gated ion channels containing voltage-sensing domains (VSDs). The VSDs are made of four membrane-spanning segments (S1 through S4), and their function is to detect changes in membrane potential in the cells. A highly conserved phenylalanine 150 (F150) is located in the S2 segment of human voltage-gated proton channels. We previously discovered that the F150 is a binding site for the open channel blocker 2GBI. Here, we show that the H_v1 VSD voltage-dependent activation requires a hydrophobic group at position F150. We perform double-mutant cycle analysis to probe interactions between F150 and positively charged arginines in the S4 segment of the channel. Our results indicate that F150 interacts with two arginines (R2 and R3) in the S4 segment and catalyzes the transfer of the S4 arginines in the process of voltage-dependent activation.

INTRODUCTION

The voltage-gated proton channel H_v1 is a member of the family of voltage-gated ion channels (Ramsey et al., 2006; Sasaki et al., 2006). H_v1 channel plays roles in the regulation of reactive oxygen species (ROS) production by the NADPH oxidase and cellular pH homeostasis (DeCoursey, 2016; Ma et al., 2022; Seredenina et al., 2015; Taylor et al., 2011; Wu et al., 2022); it was found in many cell types including airway epithelia cells (Cherny et al., 1995; DeCoursey and Cherny, 1995; Fischer, 2012; Murphy et al., 2005), sperm cells (Lishko et al., 2010; Zhao et al., 2018, 2021b), brain microglia (Peng et al., 2021; Wu et al., 2012), and cancer cells (Fernandez et al., 2016; Ribeiro-Silva et al., 2016; Wang et al., 2011, 2012, 2013), in which H_v1 activity has been implicated in the pathology of asthma, sperm capacitation, ischemic stroke, and tumor metastasis.

The voltage-gated sodium, potassium, and calcium channels are all made of a pore domain (PD) responsible for ion permeation and four non-permeable voltage-sensing domains (VSDs) detecting changes in membrane potential in the cells. The H_v1 proton channel does not have a PD and forms as a dimer consisting of two permeable VSDs held together by the coiled-coil domain (Koch et al., 2008; Lee et al., 2008; Tombola et al., 2008).

The VSDs of voltage-gated ion channels are made of four transmembrane segments (S1 through S4). A highly conserved phenylalanine is located in the S2 segment of the VSD and acts as a part of the "gating charge transfer center" (Figure 1A) (Tao et al., 2010). In the voltage-gated Shaker K^+ channel, the conserved phenylalanine (F290) was shown to interact with the positively charged residues of the S4 segment and catalyze the sequential movement of the gating charges across the electric field (Lacroix and Bezanilla, 2011; Lacroix et al., 2014; Pless et al., 2011; Schwaiger et al., 2013; Tao et al., 2010). A state model of voltage sensor transitions in the Shaker channel indicated that F290 interacts with the first positively charged residue in the fully closed VSD, and with the fifth positively charged residue when the VSD is in its depolarized conformation, suggesting a gating process consists of four transitions from the resting state to the final pore opening in the Shaker potassium channel (Tao et al., 2010). Additionally, the size of the conserved phenylalanine is important for the channel function, and the large side chain at position F290 is required to stabilize the Shaker channel depolarized VSD conformation (Lacroix et al., 2014; Tao et al., 2010).

Despite progress in the functional characterization of F290 in the Shaker K^+ channel, the role of the highly conserved phenylalanine in H_v1 VSD activation remains unclear. The H_v1 channel has a more positive half-activation voltage ($V_{1/2}$) and less number of positively charged residues in S4 segment compared with the

[1]Department of Medicine, University of Illinois at Chicago, Chicago, IL 60612, USA

[2]Department of Physiology and Biophysics, University of Illinois at Chicago, Chicago, IL 60612, USA

[3]Lead contact
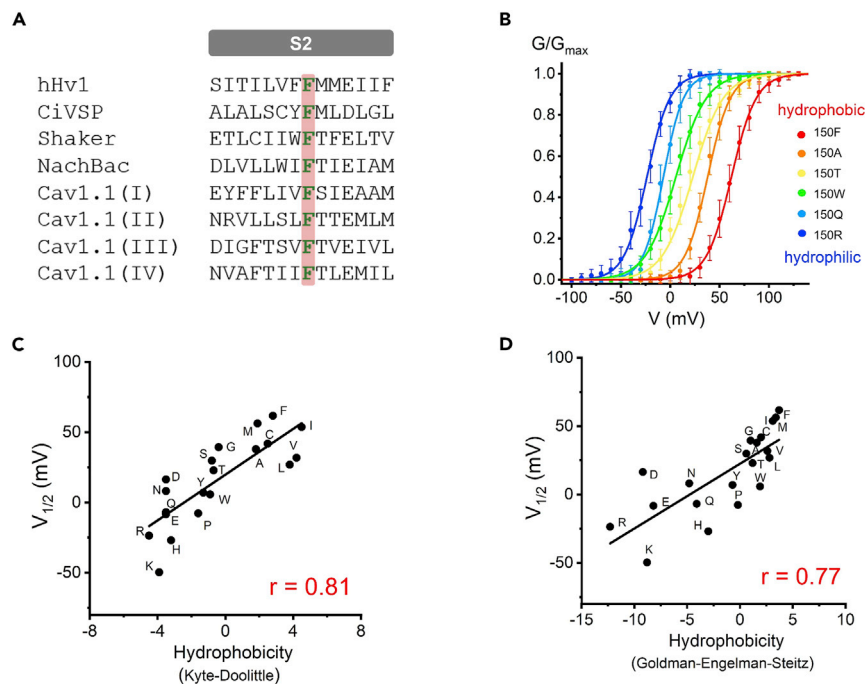
*Correspondence: hong2004@uic.edu

Figure 1. The hydrophobic group at position 150 is essential for H$_v$1 voltage-dependent activation

(A) Sequence alignment of the S2 transmembrane segment of hH$_v$1 proton channel, Shaker potassium channel, NachBac sodium channel, Ca$_v$1.1 calcium channel, and CiVSP. Highly conserved phenylalanine (F) in the S2 segments is highlighted. F corresponds to Phe150 in hH$_v$1.

(B) *G-V* curves for the hH$_v$1 proton channel F150 mutations colored from red to blue when the hydrophobicity of the substituted side chain decreases, only several F150 mutations are shown for clarity. Table S1 summarized all F150 mutations. Proton currents were recorded in HEK293 cells expressing F150 mutations, pH$_i$ = pH$_o$ = 6.0.

(C and D) The $V_{1/2}$ values obtained from *G-V* curves are plotted as a function of hydrophobicity of the substituted side chain at position F150, using either Kyte-Doolittle hydrophobicity scale (C), or Goldman-Engelman-Steitz hydrophobicity scale (D). Black lines indicate fits of the data to a linear function in (C and D), and *r* values are presented in red in each panel.

Shaker channel, indicating that the conserved phenylalanine contributes different roles in voltage-dependent activation and regulation of the VSD in specific conformations.

The highly conserved phenylalanine of the human H$_v$1 channel (hH$_v$1) is F150. We previously discovered that the side chain of F150 affects the strength of the interaction between the H$_v$1 channel and the blocker 2GBI (Hong et al., 2013, 2014), and there was a negative correlation between the side chain size at position 150 and the blocker binding affinity (Zhao et al., 2021a), suggesting that the size of F150 plays a role in 2GBI's binding.

To assess whether the side chain size of F150 regulates hH$_v$1 VSD activation as well, we introduced mutations in the F150 by substituting other 19 amino acids. We found that the hydrophobic group instead of the size of the side chain at position F150 is essential for the H$_v$1 voltage-dependent activation. We then investigated interactions between F150 and arginines in the S4 segment of the H$_v$1 channel, and the double-mutant cycle analysis characterized significantly thermodynamic couplings between F150 and R2 or R3 when the channel transits from closed state to open state. Moreover, substitutions of charge-conserving mutations at R2 or R3 destabilize the closed state or open state of the channel, respectively. We discussed a simple model consists of two states connected by one transition.

RESULTS

The hydrophobicity of phenylalanine at position 150 is essential for the voltage-dependent activation of the hH$_v$1 channel

We first introduced a small residue replacement (alanine) at position 150 of the human H$_v$1 channel (F150A) and observed that the F150A mutation shifted the conductance versus voltage relationship (*G-V* curve) to
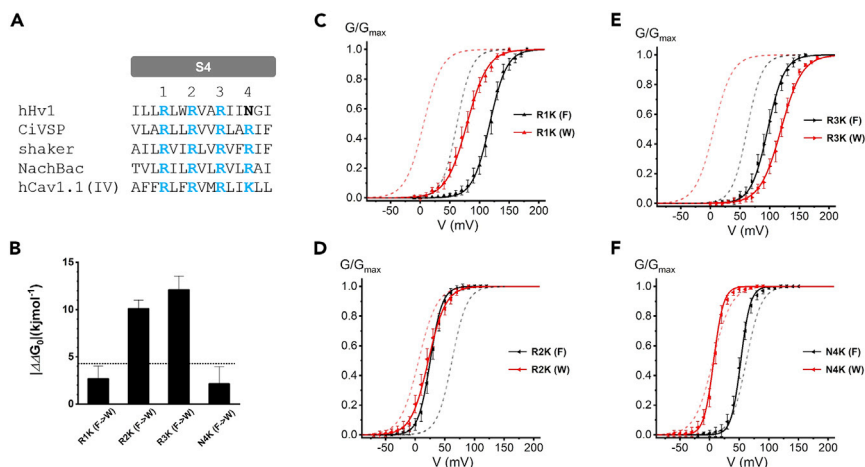
Figure 2. Double-mutant cycle analysis indicates F150 interacts with R2 and R3 during the channel activation

(A) Sequence alignment of the S4 Segment of hH$_v$1 proton channel, NachBac sodium channel, Ca$_v$1.1 calcium channel domain IV, Shaker potassium channel, and CiVSP. The positive S4 residues are highlighted in blue. In hH$_v$1, an asparagine taking the fourth position of positive S4 residues is shown in bold font. The numbers show three arginines (R1, R2, and R3) and one asparagine (N4) in the hH$_v$1 S4 segment.

(B) Summary of $|\Delta\Delta G_0|$ determined by the double-mutant cycle analysis. A significant interaction between two residues was defined as a $|\Delta\Delta G_0| > 4.2$ kJ/mol (dot line). The larger values of $|\Delta\Delta G_0|$ indicated strong interactions between F150 and R2 or R3, see STAR methods.

(C–F) Effects of mutations on the G-V relationship of the channels. Voltage-dependent channel activations were shown for R1K with 150F (R1K(F)) and R1K with 150W (R1K(W)) (C), R2K(F) and R2K(W) (D), R3K(F) and R3K(W) (E), and N4K(F) and N4K(W) (F). In (C–F), the dash line (black) represented G-V curve of WT channel (150F), and the dash line (red) represented G-V curve of F150W. Lines indicate fits of the data to a *Boltzmann* function. Proton currents were recorded in HEK293 cells expressing H$_v$1 mutations, pH$_i$ = pH$_o$ = 6.0. Data are represented as mean ± SEM.

the hyperpolarization. A substitution of bulky and aromatic residue (F150W) produced a stronger perturbation of channel activation compared with F150A. Moreover, a charged residue replacement (F150R) generated the largest G-V shift in a hyperpolarized direction among three mutations (Figures 1B and S1).

To comprehensively explore the effects of F150 on the voltage dependence of activation, we characterized all 19 mutations at position 150 (Table S1). It was shown that all mutations produced left-shifted G-V relationships that increased open state stability relative to the closed state (Figure 1B, Table S1), indicating that the nature of the side chain of phenylalanine at position 150 is required to stabilize the resting state of the channel. We next performed linear correlation analysis for the relationship between the H$_v$1 voltage dependence of activation and physicochemical properties of amino acid mutations. The voltage dependence of activation parameter V$_{1/2}$ was measured as the midpoint voltage obtained from the fitted G-V curve, and the physicochemical properties of amino acids included side chain volume and hydrophobicity (Engelman et al., 1986; Kyte and Doolittle, 1982; Zamyatnin, 1972) (Table S2).

There were no significant correlations between the V$_{1/2}$ and the size of the side chain (Figure S2). In contrast, it showed a strong linear dependence between the H$_v$1 VSD voltage dependence and hydrophobicity (Figures 1C and 1D). We tested two hydrophobicity scales Kyte-Doolittle (Kyte and Doolittle, 1982) and Goldman-Engelman-Steitz (Engelman et al., 1986), and the V$_{1/2}$ is correlated with both of hydrophobicity scales. The data showed that the V$_{1/2}$ is associated with the hydrophobicity at position 150, and a hydrophobic residue at position F150 is important for the channel function.

Effects of mutations at position 150 depend on the positive residues in the S4 transmembrane segment

The highly conserved phenylalanine has been reported to interact with S4 charges to control the VSD gating (Figure 2A). In the Shaker channel, the effect of phenylalanine to tryptophan mutation (F290W) was associated with charged residue at position 5 (K5 in the Shaker S4) when the Shaker K$^+$ channel VSD

is in the open conformation (Tao et al., 2010). Since F150 mutations have strong effects on the voltage-dependent activation of the H_v1 channel, we wondered whether we could identify interactions similar to those between F290 and S4 charges in the Shaker channel that also occur in the H_v1 channel.

A double-mutant cycle analysis has been used to probe residues' interaction between transmembrane segments in the channel (Chamberlin et al., 2014). Similar approaches were introduced to investigate the effects of combining the F150W and charge-conserving S4 mutations (Figure 2). The H_v1 channel has 3 arginines (R1, R2, and R3) in the S4 segment. An asparagine (N4) takes the fourth position of positive S4 residues in the VSDs of other channels (Figure 2A), and we generated a mutation at this position as well in the human H_v1 channel.

The *G-V* curves of the F150 mutation (F150W) with or without S4 segment mutations (R1K, R2K, R3K, and N4K) were summarized in Figures 2C–2F. For each mutation, the *G-V* curve was fitted with the *Boltzmann* equation, and $V_{1/2}$ and k slope factors were then determined and used to calculate the ΔG_0, which is the free energy difference between the closed and open states of the activation. The $|\Delta\Delta G_0|$ (i.e., coupling ΔG_0 value) between two position mutations was determined by the thermodynamic coupling analysis as previously explained (Li-Smerin et al., 2000). The significant interaction between two residues was defined as a $|\Delta\Delta G_0| > 4.2$ kJ/mol (1 kcal/mol) (Cheng et al., 2013; Zhang et al., 2005).

The $|\Delta\Delta G_0|$ values determined by the double-mutant cycle analysis were reported in Figure 2B. We observed that the combinations F150W-R1K and F150W-N4K had $|\Delta\Delta G_0|$ values smaller than 4.2 kJ/mol, indicating that there are no thermodynamic couplings between F150 and R1 or N4. In contrast, the combinations F150W-R2K and F150W-R3K dramatically increased the $|\Delta\Delta G_0|$, and the values were 10.1 and 12.1 kJ/mol, respectively, both were substantially higher than the ones for F150W-R1K and F150W-N4K (Figure 2B, Table S3). We then investigated residues near the F150 (F149 and M151), and the combinations F149W-R2K, F149W-R3K, M151W-R2K, and M151W-R3K all showed smaller $|\Delta\Delta G_0|$ compared with F150W-R2K and F150W-R3K (Figure S3). This strongly suggests that F150 is able to form functional interactions with R2 or R3 during the voltage-dependent activation, and serve as a part of the gating charge transfer center in the H_v1 channel.

We previously used an open channel blocker to probe that the F150 and D112, a residue crucial for the proton selectivity of the channel, are located close to each other (Hong et al., 2014). We next investigated if the D112 affects the interactions between F150 and S4 arginines. The combination F150 and D112 mutation (F150W-D112E) generated a $|\Delta\Delta G_0|$ value (6.0 kJ/mol) larger than 4.2 kJ/mol, indicating an interaction between F150 and D112 (Figure S4). The significantly thermodynamic coupling between D112 and F150 was consistent with the results that D112E mutation affected F150 interactions with R2 or R3 (Figure S5).

F150 interacts with R2 and R3 to stabilize the closed and open states of the H_v1 channel

The VSD activation is a process that S4 segment positively charged amino acids move from inside to outside of the membrane field (Tombola et al., 2006). As the mutant cycle analysis showed that F150 interacts with both R2 and R3 during the channel activation (a process by which the channel transitions between its closed and open states), we propose that F150 interacts with R2 to stabilize the closed state of the channel, and when the channel is depolarized, the R3 reaches the binding site and interacts with F150 to stabilize the open state of the H_v1 VSD.

A charge-conserving mutation at R2 (R2K) was introduced to the H_v1 channel (Figure 3). The R2K mutation shifted the *G-V* curve to the hyperpolarized direction with faster activation kinetics (Figures 3C and S6). The channel closing time constant τ_{deact} values were determined, and R2K mutation took longer time to close compared with WT (Figures 3B and 3D). The hyperpolarized-shifted *G-V* curve, decreased ΔG_0, and the slower rate of closure indicate that the replacement of lysine at position 2 (R2K) destabilizes the closed state of the channel. This suggests that the endogenous residue (arginine) at position 2 increases the relative stability of the closed conformation.

The effects of charge-conserving mutation at the R3 (R3K) were further investigated (Figure 4). In contrast to R2K, the R3K shifted the *G-V* relationship to the depolarized direction (Figure 4C), indicating that the R3K mutation made the channel more difficult to open and did not favor the open conformation. The R3K had a
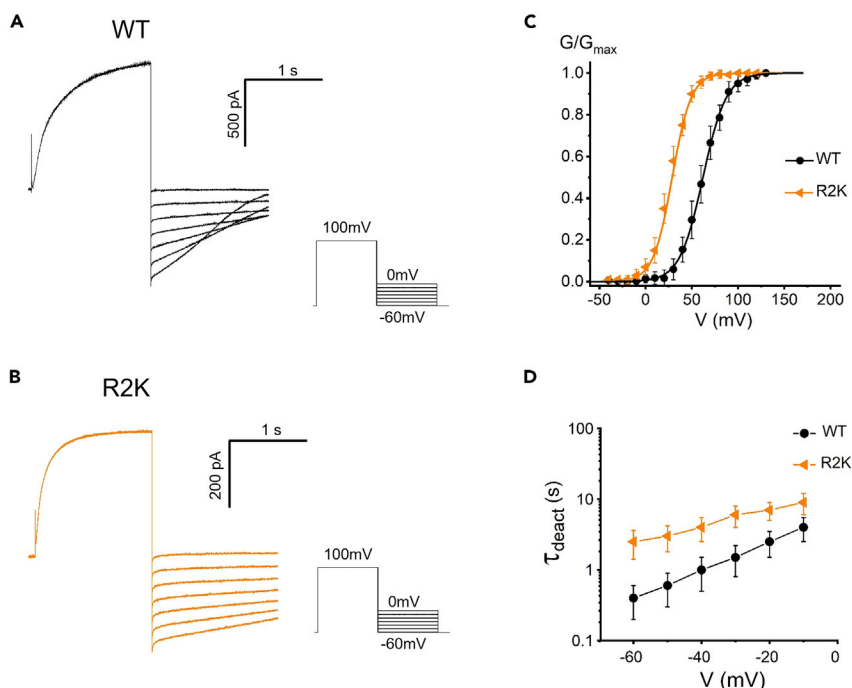
Figure 3. Effects of charge conserving mutation of R2 on the closed state of the channel

(A and B) Representative tail currents recorded from WT (A) or R2K (B). The tail currents were elicited by a prepulse to 100 mV, in 10 mV decrements from 0 to −60 mV.

(C) The R2K mutation negatively shifted the G-V relationship of the channel. Lines indicate fits of the data to a *Boltzmann* function.

(D) The deactivation (channel closing) time constant τ_{deact} in WT or R2K mutation. τ_{deact} was obtained from *exponential* fit to the tail currents. Proton currents were recorded in HEK293 cells expressing H_v1 mutations, $pH_i = pH_o = 6.0$. Data are represented as mean $\pm$ SEM.

depolarized-shifted G-V relationship, increased ΔG_0, and faster deactivation kinetics (Figure S7), which is indicative of a destabilized open state relative to the closed state. This is consistent with the results that R3K mutation significantly delayed the activation kinetics (Figure 4B), and it altered the opening time constant τ_{act} increasing the values at given membrane potentials (Figure 4D). These results indicated that the function of native arginine at position 3 is to stabilize the open channel, and mutation at R3 (R3K) strongly perturbs the stability of the open state. The spatial proximity between F150 and R3 was further assessed by cysteine pairs crosslinking; an approach that used Cd^{2+} to probe for cysteine-cysteine distances has been previously applied on other channel (Campos et al., 2007). Here, we introduced double cysteine mutations (F150C-R3C) in the H_v1 channel expressing in *Xenopus* oocytes. The current carried by F150C-R3C cysteine pairs was remarkably decreased by intracellular Cd^{2+} compared with the currents carried by single cysteine mutation F150C or R3C (Figure S8), indicating a formation of Cd^{2+} bridge between the two residue pairs.

Model of H_v1 VSD transitions

To describe the effects of R2K and R3K on the H_v1 VSD voltage-dependent activation, we proposed a simple-state model of H_v1 VSD transitions. We assumed that H_v1 proton current permeation corresponds to the translocation of the voltage-sensing residues in the S4 segment, and that the H_v1 open pore correlates with the condition in which H_v1 VSD is open. The model is comprised of one closed state and one open state, each state occupying an energy well. The transition rates depend on the height of the energy barrier between closed and open states (Figure 5).

In the model, the effect of the R2K mutation on the channel, which is closed state destabilization, was satisfied by decreasing the relative depth of the energy well for the "Close" state and increasing the energy barrier for the Open -> Close transition to allow for the slower deactivation (orange lines in Figure 5A).
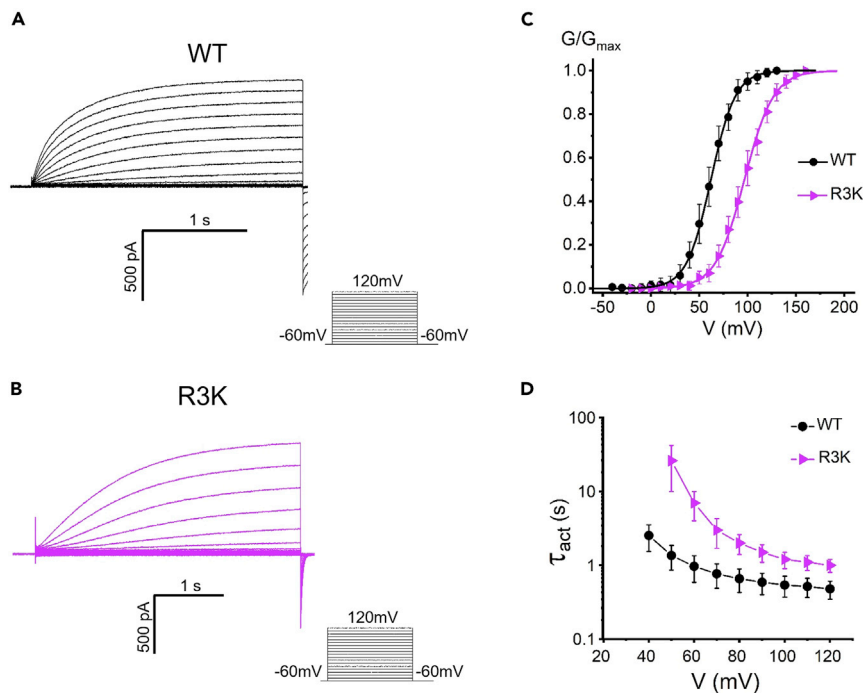
Figure 4. Effects of charge conserving mutation of R3 on the open state of the channel

(A and B) Representative rising currents recorded from WT (A) or R3K (B). Currents were measured from a holding potential of −60 mV to test potentials ranging between −60 and +120 mV in 10 mV steps.

(C) The R3K mutation positively shifted the *G-V* relationship of the channel. Lines indicate fits of the data to a *Boltzmann* function.

(D) The channel opening time constant τ_{act} in WT or R3K mutation. τ_{act} was obtained from *exponential* fit to rising currents. Proton currents were recorded in HEK293 cells expressing H_v1 mutations, $pH_i = pH_o = 6.0$. Data are represented as mean ± SEM.

A smaller ΔG_0 for R2K was consistent with decreased activation kinetics (E_{act}(R2K)) (Figure S6B) and increased deactivation kinetics (E_{deact}(R2K)) (Figure 3D).

The effects of the R3K mutation on the open state of the channel could also be described using this model, and R3K destabilizing the open state could be satisfied by decreasing the relative depth of the energy well for the "Open" state and increasing the energy barrier for the Close - > Open transition to interpret the slower activation (purple lines in Figure 5B). A larger ΔG_0 for R3K was consistent with increasing the height of the energy well (increased E_{act}(R3K), Figure 4D) and decreasing the depth of the energy well for the open state (decreased E_{deact}(R3K)) (Figure S7B).

DISCUSSION

In the Shaker potassium channel, the large side chain at position F290 is required to stabilize the depolarized VSD conformation (Lacroix et al., 2014); the role of the side chain size at position F290 in Shaker channel was supported by discoveries that the size of unnatural amino acid analogs of phenylalanine at position 290 was negatively correlated with the voltage-dependent channel activation curves (Pless et al., 2011; Tao et al., 2010).

In contrast to the Shaker channel, the highly conserved phenylalanine of the H_v1 channel (F150) exhibited distinctive features. We determined the *G-V* curves of F150 mutations and analyzed the effects of physico-chemical properties of F150 mutations on the voltage-dependent activation. There were no significant correlations between the size of side chain and the midpoint $V_{1/2}$ values in H_v1. Strikingly, replacements of hydrophilic residues at position 150 consistently shift the *G-V* curve toward more negative voltages, indicating that stabilization of the resting H_v1 VSD conformation requires a hydrophobic group at position F150. A recent finding that increasing the hydrophilicity of the H_v1 hydrophobic gasket region including
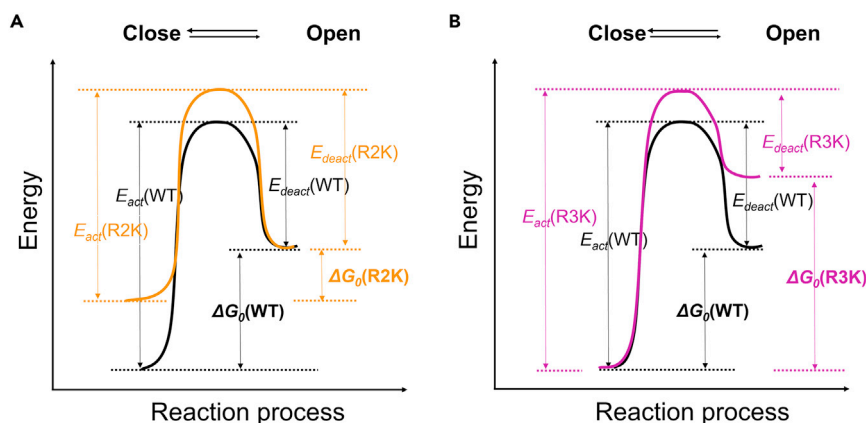
Figure 5. State model of H$_v$1 VSD transitions

(A) The black lines represent the voltage-dependent activation for wild-type H$_v$1 channels, and orange lines are changes mediated by the R2K mutation. Destabilization of closed state caused by R2K is consistent with decreasing the relative depth of the energy well for the "Close" state and increasing the energy barrier for the Open -> Close transition to allow for the slower deactivation. And the smaller ΔG_0 for R2K is satisfied by decreased activation kinetics $E_{act}(R2K)$ and increased deactivation kinetics $E_{deact}(R2K)$.

(B) The similar reaction process can be interpreted for the effects of R3K mutation on the open state. Purple lines are changes mediated by the R3K mutation. Destabilization of the open state caused by R3K is achieved by decreasing the relative depth of the energy well for the "Open" state and increasing the energy barrier for the Close -> Open transition to account for the slower activation. The larger ΔG_0 for R3K is consistent with increased activation kinetics $E_{act}(R3K)$ and decreased deactivation kinetics $E_{deact}(R3K)$.

F150 facilitated channel opening supports this conclusion (Banh et al., 2019). The presence of the hydrophobic side chain at position 150 might play an essential role in preventing protons permeating the VSD when the channel is in closed conformation.

Although the side chain size at position F150 is not correlated with the H$_v$1 VSD voltage-dependent activation, it strongly affects the H$_v$1 pharmacology. Mutations at position F150 have been shown to influence the strength of the interaction between the channel and the H$_v$1 blocker 2GBI (Hong et al., 2013, 2014). A replacement of small amino acid alanine (F150A) generated over 350-fold increase in binding affinity for the blocker, whereas substitution of bulky residue at position 150 (F150W) reduced the binding affinity of the 2GBI (Hong et al., 2013). These suggest that the mechanism by which F150 mutations alter the blocker binding is distinct from the mechanism by which they alter the movement of the voltage sensor. We conclude that the nature of the side chain of phenylalanine at position 150 has differential effects on the channel function: the size of phenylalanine plays a key role in blocker binding, while the hydrophobicity of phenylalanine is essential for the channel voltage-dependent activation.

Previous studies on the VSDs of voltage-gated potassium channels revealed that the conserved phenylalanine interacts with different S4 arginines in different conformations (Henrion et al., 2012). In the Shaker channel, F290 was proposed to interact with the first positively charged residue in the closed state, and with the fifth positively charged residue in the channel open conformation, suggesting a gating process consists of four transitions from the resting state to the final pore opening in the Shaker potassium channel (Henrion et al., 2012; Tao et al., 2010).

Compared with the Shaker channel, the S4 movement in H$_v$1 channel is shorter. Two different models of H$_v$1 voltage-dependent activation have been proposed (DeCoursey, 2015; Larsson, 2020). In the "three-click" model, the S4 segment moves three turns of the helix upward and three arginines all move outward past the hydrophobic gasket in the VSD (Gonzalez et al., 2010). In the "one-click" model, there is only one transition and the S4 moves one turn of the helix upward (Li et al., 2015).

We applied double-mutant cycle analysis to probe interactions between the conserved phenylalanine F150 and arginines in the S4 segment, and found that there are significantly thermodynamic couplings between F150 and R2 or R3 when the channel transits between closed and open conformations.
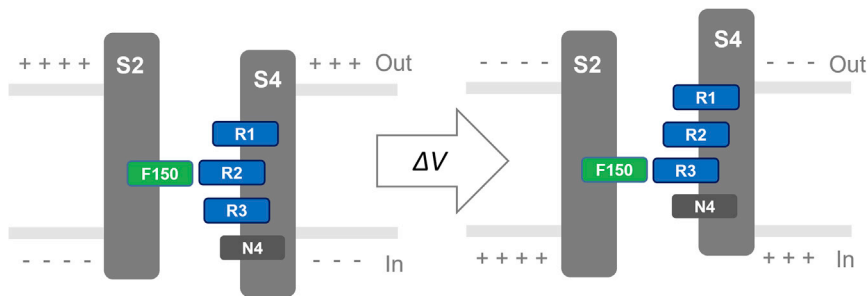
Figure 6. Schematic showing the proposed interactions between F150 and S4 gating charges in the S4 segment
The hydrophobic F150 interacts with R2 to stabilize the closed state of the channel (left panel). When the channel is depolarized, the R3 reaches the binding site interacting with F150 to stabilize the open state of the channel (right panel).

Our findings indicated that F150 is close to the arginine at position 2 (R2) in the resting state, which is consistent with the crystal structure of the closed conformation of the H_v1-VSP chimera (Takeshita et al., 2014). Substitution of a charge-conserving mutation at R2 (R2K) produced hyperpolarized shifts of the G-V curve (Figure 3), and this mutation took less time to activate and much longer time to close, indicating that the R2K strongly destabilizes the closed state relative to the open state of the channel. This might be due to the fact that the charged side chain of lysine (K) is shorter than arginine (R), and F150 could not effectively interact with the lysine at position 2 (R2K) in order to stabilize the closed conformation.

To date, the crystal structure of the open state of the H_v1 channel has not yet been achieved. We previously used an open channel blocker 2GBI to probe a locally structural information when the H_v1 channel opens (Hong et al., 2014); we characterized that the binding environment of 2GBI is a cluster of tightly packed residues including F150 and R3 within the H_v1 VSD. This suggested that in the H_v1 open conformation, F150 and R3 are packed in space and likely interact with each other. The results in the present study were consistent with this conclusion. The R3K mutation markedly slowed the process of channel opening (Figure 4), suggesting that it perturbed the open conformation of the channel. The depolarized shift of the G-V produced by R3K showed that more energies are required to push the lysine (K) at position 3 into the binding site to interact with F150, suggesting that the native arginine (R) binds more tightly relative to lysine (K) in the presence of phenylalanine at position 150, which made the voltage sensor to be stabilized in its open conformation. Moreover, the interaction between F150 and R3 was supported by the results of cysteine pairs cross-links (Figure S8).

We propose a simple model consists of two states (closed and open) connected by one transition: The F150 interacting with R2 stabilizes the closed state of the channel. When depolarized, the R3 moves sequentially upward to interact with F150 stabilizing the open state of the channel (Figure 6).

Although our results indicated that F150 does not interact with R1, the R1 mutations have been shown to modulate the H_v1 channel voltage-dependent activation and facilitate channel opening with faster activation kinetics (Ramsey et al., 2006; Sasaki et al., 2006). Previous studies in NaChBac channel revealed that the positive residue R1 of the S4 segment interacted with a negative residue E43 at the extracellular end of the S1 segment to form charge-charge interaction stabilizing the channel in resting state (DeCaen et al., 2011; Yarov-Yarovoy et al., 2012). The E43 in NaChBac corresponds to the E119 in human H_v1 channel. Mutations at R1 in the H_v1 proton channel likely generated a perturbation of the charge-charge interaction between R1 and E119 and destabilized the resting state of the channel, reducing an energy barrier for the channel activation, accounting for faster activations in the R1 mutations of the H_v1 channel.

The physicochemical basis for interaction between F150 and S4 arginines in the H_v1 channel is potentially associated with cation-π binding. In Shaker channel, cation-π interaction was found to stabilize the interaction between S4 positive-charged residue K374 (K5) and F290W. Fluorine modifications at F290W produced a stepwise right-shift in the G-V of the Shaker channel, indicating that the electronegative surface potential of aromatic residue contributes to a cation-π interaction with positive charged residue (Pless et al., 2011). In the H_v1 channel, the aromatic side chain of F150 has been previously shown to contribute a cation-π interaction between the F150 and blocker 2GBI (Zhao et al., 2021a). A similar interaction might

be present in the H_v1 channel when F150 interacts with S4 positive-charged residues during the channel activation. The aromatic ring of F150 catalyzes the S4 movement potentially through the electrostatic cation-π interaction with the R2 or R3. A detailed mechanism underlying the interaction remains to be explored in future work.

Taken together, our results identify a role for F150 in the regulation of H_v1 channel function. We show that the highly conserved phenylalanine of the H_v1 channel exhibits different features and that the hydrophobicity of phenylalanine is essential for channel voltage-dependent activation. The F150 functionally interacts with arginines at positions 2 and 3 in the S4 segment and catalyzes the transfer of the S4 arginines in the process of voltage sensing. The voltage-gated proton channel H_v1 has been associated with ROS generation and regulation of pH homeostasis. Understanding how H_v1 proton channel activity is manipulated by transmembrane potential will shed light on the instructions in creation of reagents targeting this channel, and therapeutics to rationally modulation of H_v1 activity.

Limitations of the study

The study showed that the conserved phenylalanine F150 in the human H_v1 channel interacts with two S4 arginines when the channel transits between closed and open conformations. Although the data in our study supported that in the H_v1 open conformation, R3 and F150 interact with each other to stabilize the open state, so far, the structure of the activated state of the H_v1 channel is not available to justify the model. Additionally, the detailed mechanism underlying the interaction between the hydrophobic phenylalanine and positively charged arginines in the H_v1 channel remains to be explored in future work.

STAR★METHODS

Detailed methods are provided in the online version of this paper and include the following:

- KEY RESOURCES TABLE
- RESOURCE AVAILABILITY
  - Lead contact
  - Materials availability
  - Data and code availability
- EXPERIMENTAL MODEL AND SUBJECT DETAILS
  - Cell culture
- METHOD DETAILS
  - Electrophysiological measurements and analysis
  - Mutant cycle analysis
- QUANTIFICATION AND STATISTICAL ANALYSIS

AUTHOR CONTRIBUTIONS

L.H. conceived the project and designed the experiments. X.W., L.Z., and L.H. performed experiments and data analysis. X.W. and L.H. wrote the manuscript.

DECLARATION OF INTERESTS

The authors declare no competing interests.

REFERENCES

Banh, R., Cherny, V.V., Morgan, D., Musset, B., Thomas, S., Kulleperuma, K., Smith, S.M.E., Pomès, R., and DeCoursey, T.E. (2019). Hydrophobic gasket mutation produces gating pore currents in closed human voltage-gated proton channels. Proc. Natl. Acad. Sci. USA 116, 18951–18961.

Campos, F.V., Chanda, B., Roux, B., and Bezanilla, F. (2007). Two atomic constraints unambiguously position the S4 segment relative to S1 and S2 segments in the closed state of Shaker K channel. Proc. Natl. Acad. Sci. USA 104, 7904–7909.

Chamberlin, A., Qiu, F., Rebolledo, S., Wang, Y., Noskov, S.Y., and Larsson, H.P. (2014). Hydrophobic plug functions as a gate in voltage-gated proton channels. Proc. Natl. Acad. Sci. USA 111, E273–E282.

Cheng, Y.M., Hull, C.M., Niven, C.M., Qi, J., Allard, C.R., and Claydon, T.W. (2013). Functional interactions of voltage sensor charges with an S2 hydrophobic plug in hERG channels. J. Gen. Physiol. 142, 289–303.

Cherny, V.V., Markin, V.S., and DeCoursey, T.E. (1995). The voltage-activated hydrogen ion conductance in rat alveolar epithelial cells is determined by the pH gradient. J. Gen. Physiol. 105, 861–896.

DeCaen, P.G., Yarov-Yarovoy, V., Scheuer, T., and Catterall, W.A. (2011). Gating charge interactions with the S1 segment during activation of a Na+ channel voltage sensor. Proc. Natl. Acad. Sci. USA 108, 18825–18830.

DeCoursey, T.E. (2015). Structural revelations of the human proton channel. Proc. Natl. Acad. Sci. USA 112, 13430–13431.

DeCoursey, T.E. (2016). The intimate and controversial relationship between voltage-gated proton channels and the phagocyte NADPH oxidase. Immunol. Rev. 273, 194–218.

DeCoursey, T.E., and Cherny, V.V. (1995). Voltage-activated proton currents in membrane patches of rat alveolar epithelial cells. J. Physiol. 489, 299–307.

Engelman, D.M., Steitz, T.A., and Goldman, A. (1986). Identifying nonpolar transbilayer helices in amino acid sequences of membrane proteins. Annu. Rev. Biophys. Biophys. Chem. 15, 321–353.

Fernández, A., Pupo, A., Mena-Ulecia, K., and Gonzalez, C. (2016). Pharmacological modulation of proton channel Hv1 in cancer therapy: future perspectives. Mol. Pharmacol. 90, 385–402.

Fischer, H. (2012). Function of proton channels in Lung Epithelia. Wiley Interdisc Rev. Membr. Transp. Signal. 1, 247–258.

Gonzalez, C., Koch, H.P., Drum, B.M., and Larsson, H.P. (2010). Strong cooperativity between subunits in voltage-gated proton channels. Nat. Struct. Mol. Biol. 17, 51–56.

Henrion, U., Renhorn, J., Börjesson, S.I., Nelson, E.M., Schwaiger, C.S., Bjelkmar, P., Wallner, B., Lindahl, E., and Elinder, F. (2012). Tracking a complete voltage-sensor cycle with metal-ion bridges. Proc. Natl. Acad. Sci. USA 109, 8552–8557.

Hong, L., Kim, I.H., and Tombola, F. (2014). Molecular determinants of Hv1 proton channel inhibition by guanidine derivatives. Proc. Natl. Acad. Sci. USA 111, 9971–9976.

Hong, L., Pathak, M.M., Kim, I.H., Ta, D., and Tombola, F. (2013). Voltage-sensing domain of voltage-gated proton channel Hv1 shares mechanism of block with pore domains. Neuron 77, 274–287.

Koch, H.P., Kurokawa, T., Okochi, Y., Sasaki, M., Okamura, Y., and Larsson, H.P. (2008). Multimeric nature of voltage-gated proton channels. Proc. Natl. Acad. Sci. USA 105, 9111–9116.

Kyte, J., and Doolittle, R.F. (1982). A simple method for displaying the hydropathic character of a protein. J. Mol. Biol. 157, 105–132.

Lacroix, J.J., and Bezanilla, F. (2011). Control of a final gating charge transition by a hydrophobic residue in the S2 segment of a K+ channel voltage sensor. Proc. Natl. Acad. Sci. USA 108, 6444–6449.

Lacroix, J.J., Hyde, H.C., Campos, F.V., and Bezanilla, F. (2014). Moving gating charges through the gating pore in a Kv channel voltage sensor. Proc. Natl. Acad. Sci. USA 111, E1950–E1959.

Larsson, H.P. (2020). Zn2+ to probe voltage-gated proton (Hv1) channels. J. Gen. Physiol. 152. e202012725.

Lee, S.Y., Letts, J.A., and Mackinnon, R. (2008). Dimeric subunit stoichiometry of the human voltage-dependent proton channel Hv1. Proc. Natl. Acad. Sci. USA 105, 7692–7695.

Li-Smerin, Y., Hackos, D.H., and Swartz, K.J. (2000). A localized interaction surface for voltage-sensing domains on the pore domain of a K+ channel. Neuron 25, 411–423.

Li, Q., Shen, R., Treger, J.S., Wanderling, S.S., Milewski, W., Siwowska, K., Bezanilla, F., and Perozo, E. (2015). Resting state of the human proton channel dimer in a lipid bilayer. Proc. Natl. Acad. Sci. USA 112, E5926–E5935.

Lishko, P.V., Botchkina, I.L., Fedorenko, A., and Kirichok, Y. (2010). Acid extrusion from human spermatozoa is mediated by flagellar voltage-gated proton channel. Cell 140, 327–337.

Ma, J., Gao, X., Li, Y., DeCoursey, T.E., Shull, G.E., and Wang, H.S. (2022). The HVCN1 voltage-gated proton channel contributes to pH regulation in canine ventricular myocytes. J. Physiol. 600, 2089–2103.

Murphy, R., Cherny, V.V., Morgan, D., and DeCoursey, T.E. (2005). Voltage-gated proton channels help regulate pHi in rat alveolar epithelium. Am. J. Physiol. Lung Cell Mol. Physiol. 288, L398–L408.

Peng, J., Yi, M.H., Jeong, H., McEwan, P.P., Zheng, J., Wu, G., Ganatra, S., Ren, Y., Richardson, J.R., Oh, S.B., and Wu, L.J. (2021). The voltage-gated proton channel Hv1 promotes microglia-astrocyte communication and neuropathic pain after peripheral nerve injury. Mol. Brain 14, 99.

Pless, S.A., Galpin, J.D., Niciforovic, A.P., and Ahern, C.A. (2011). Contributions of counter-charge in a potassium channel voltage-sensor domain. Nat. Chem. Biol. 7, 617–623.

Ramsey, I.S., Moran, M.M., Chong, J.A., and Clapham, D.E. (2006). A voltage-gated proton-selective channel lacking the pore domain. Nature 440, 1213–1216.

Ribeiro-Silva, L., Queiroz, F.O., da Silva, A.M.B., Hirata, A.E., and Arcisio-Miranda, M. (2016). Voltage-gated proton channel in human glioblastoma multiforme cells. ACS Chem. Neurosci. 7, 864–869.

Sasaki, M., Takagi, M., and Okamura, Y. (2006). A voltage sensor-domain protein is a voltage-gated proton channel. Science 312, 589–592.

Schwaiger, C.S., Liin, S.I., Elinder, F., and Lindahl, E. (2013). The conserved phenylalanine in the K+ channel voltage-sensor domain creates a barrier with unidirectional effects. Biophys. J. 104, 75–84.

Seredenina, T., Demaurex, N., and Krause, K.H. (2015). Voltage-gated proton channels as novel drug targets: from NADPH oxidase regulation to sperm biology. Antioxid. Redox Signal. 23, 490–513.

Takeshita, K., Sakata, S., Yamashita, E., Fujiwara, Y., Kawanabe, A., Kurokawa, T., Okochi, Y., Matsuda, M., Narita, H., Okamura, Y., and Nakagawa, A. (2014). X-ray crystal structure of voltage-gated proton channel. Nat. Struct. Mol. Biol. 21, 352–357.

Tao, X., Lee, A., Limapichat, W., Dougherty, D.A., and MacKinnon, R. (2010). A gating charge transfer center in voltage sensors. Science 328, 67–73.

Taylor, A.R., Chrachri, A., Wheeler, G., Goddard, H., and Brownlee, C. (2011). A voltage-gated H+ channel underlying pH homeostasis in calcifying coccolithophores. PLoS Biol. 9, e1001085.

Tombola, F., Pathak, M.M., and Isacoff, E.Y. (2006). How does voltage open an ion channel? Annu. Rev. Cell Dev. Biol. 22, 23–52.

Tombola, F., Ulbrich, M.H., and Isacoff, E.Y. (2008). The voltage-gated proton channel Hv1 has two pores, each controlled by one voltage sensor. Neuron 58, 546–556.

Wang, Y., Li, S.J., Pan, J., Che, Y., Yin, J., and Zhao, Q. (2011). Specific expression of the human voltage-gated proton channel Hv1 in highly metastatic breast cancer cells, promotes tumor progression and metastasis. Biochem. Biophys. Res. Commun. 412, 353–359.

Wang, Y., Li, S.J., Wu, X., Che, Y., and Li, Q. (2012). Clinicopathological and biological significance of human voltage-gated proton channel Hv1 protein overexpression in breast cancer. J. Biol. Chem. 287, 13877–13888.

Wang, Y., Wu, X., Li, Q., Zhang, S., and Li, S.J. (2013). Human voltage-gated proton channel hv1: a new potential biomarker for diagnosis and

prognosis of colorectal cancer. PLoS One *8*, e70550.

Wu, L.J., Wu, G., Akhavan Sharif, M.R., Baker, A., Jia, Y., Fahey, F.H., Luo, H.R., Feener, E.P., and Clapham, D.E. (2012). The voltage-gated proton channel Hv1 enhances brain damage from ischemic stroke. Nat. Neurosci. *15*, 565–573.

Wu, X., Li, Y., Maienschein-Cline, M., Feferman, L., Wu, L., and Hong, L. (2022). RNA-seq analyses reveal roles of the HVCN1 proton channel in cardiac pH homeostasis. Front. Cell Dev. Biol. *10*, 860502.

Yarov-Yarovoy, V., DeCaen, P.G., Westenbroek, R.E., Pan, C.Y., Scheuer, T., Baker, D., and Catterall, W.A. (2012). Structural basis for gating charge movement in the voltage sensor of a sodium channel. Proc. Natl. Acad. Sci. USA *109*, E93–E102.

Zamyatnin, A.A. (1972). Protein volume in solution. Prog. Biophys. Mol. Biol. *24*, 107–123.

Zhang, M., Liu, J., Jiang, M., Wu, D.M., Sonawane, K., Guy, H.R., and Tseng, G.N. (2005). Interactions between charged residues in the transmembrane segments of the voltage-sensing domain in the hERG channel. J. Membr. Biol. *207*, 169–181.

Zhao, C., Hong, L., Galpin, J.D., Riahi, S., Lim, V.T., Webster, P.D., Tobias, D.J., Ahern, C.A., and Tombola, F. (2021a). HIFs: new arginine mimic inhibitors of the Hv1 channel with improved VSD-ligand interactions. J. Gen. Physiol. *153*. e202012832.

Zhao, R., Dai, H., Arias, R.J., De Blas, G.A., Orta, G., Pavarotti, M.A., Shen, R., Perozo, E., Mayorga, L.S., Darszon, A., and Goldstein, S.A.N. (2021b). Direct activation of the proton channel by albumin leads to human sperm capacitation and sustained release of inflammatory mediators by neutrophils. Nat. Commun. *12*, 3855.

Zhao, R., Kennedy, K., De Blas, G.A., Orta, G., Pavarotti, M.A., Arias, R.J., de la Vega-Beltrán, J.L., Li, Q., Dai, H., Perozo, E., et al. (2018). Role of human Hv1 channels in sperm capacitation and white blood cell respiratory burst established by a designed peptide inhibitor. Proc. Natl. Acad. Sci. USA *115*, E11847–E11856.

STAR★METHODS

KEY RESOURCES TABLE

REAGENT or RESOURCE	SOURCE	IDENTIFIER
Bacterial and virus strains		
Escherichia coli (MAX Efficiency Stbl2 Competent Cells)	Invitrogen	Cat# 10268019
Chemicals, peptides, and recombinant proteins		
Opti-MEM Reduced Serum Medium	GIBCO	Cat# 31985070
Dulbecco modified Eagle's medium	GIBCO	Cat# 12430054
Lipofectamine 3000 Transfection Reagent	Invitrogen	Cat# L3000075
NheI restriction enzyme	New England Biolabs	Cat# R3131S
mMESSAGE mMACHIN T7 Transcription Kit	Ambion	Cat# AM1344
Experimental models: Cell lines		
human-derived renal epithelial (HEK-293) cells	Sigma-Aldrich	Cat# 85120602
Xenopus oocytes	Ecocyte Bioscience	N/A
Oligonucleotides		
Custom-designed primers for mutagenesis of hHv1 constructs (see Table S4)	IDT-DNA Technologies	N/A
Recombinant DNA		
hHv1-pNICE	This paper	N/A
eGFP-pNICE	This paper	N/A
hHv1 F150A-pNICE	This paper	N/A
hHv1 F150C-pNICE	This paper	N/A
hHv1 F150D-pNICE	This paper	N/A
hHv1 F150E-pNICE	This paper	N/A
hHv1 F150G-pNICE	This paper	N/A
hHv1 F150H-pNICE	This paper	N/A
hHv1 F150I-pNICE	This paper	N/A
hHv1 F150K-pNICE	This paper	N/A
hHv1 F150L-pNICE	This paper	N/A
hHv1 F150M-pNICE	This paper	N/A
hHv1 F150N-pNICE	This paper	N/A
hHv1 F150P-pNICE	This paper	N/A
hHv1 F150Q-pNICE	This paper	N/A
hHv1 F150R-pNICE	This paper	N/A
hHv1 F150S-pNICE	This paper	N/A
hHv1 F150T-pNICE	This paper	N/A
hHv1 F150V-pNICE	This paper	N/A
hHv1 F150W-pNICE	This paper	N/A
hHv1 F150Y-pNICE	This paper	N/A
hHv1 R1K(R205K)-pNICE	This paper	N/A
hHv1 R2K(R208K)-pNICE	This paper	N/A
hHv1 R3K(R211K)-pNICE	This paper	N/A
hHv1 N4K(N214K)-pNICE	This paper	N/A
hHv1 F150W-R1K-pNICE	This paper	N/A

Continued

REAGENT or RESOURCE	SOURCE	IDENTIFIER
hHv1 F150W-R2K-pNICE	This paper	N/A
hHv1 F150W-R3K-pNICE	This paper	N/A
hHv1 F150W-N4K-pNICE	This paper	N/A
hHv1 D112E-pNICE	This paper	N/A
hHv1 D112E-F150W-pNICE	This paper	N/A
hHv1 D112E-F150W-R2K-pNICE	This paper	N/A
hHv1 D112E-F150W-R3K-pNICE	This paper	N/A
hHv1 F149W-pNICE	This paper	N/A
hHv1 F149W-R2K-pNICE	This paper	N/A
hHv1 F149W-R3K-pNICE	This paper	N/A
hHv1 M151W-pNICE	This paper	N/A
hHv1 M151W-R2K-pNICE	This paper	N/A
hHv1 M151W-R3K-pNICE	This paper	N/A
hHv1 F150C-pGEMHE	This paper	N/A
hHv1 R3C(R211C)-pGEMHE	This paper	N/A
hHv1 F150C-R3C-pGEMHE	This paper	N/A
Software and algorithms		
pClamp11 software	Molecular Devices	https://www.moleculardevices.com/
Excel	Microsoft Office	N/A
Illustrator	Adobe	https://www.adobe.com/products/illustrator.html
Origin	OriginLab	https://www.originlab.com/
BioEdit	Informer Technologies, Inc.	https://bioedit.software.informer.com/

RESOURCE AVAILABILITY

Lead contact

Further information and requests for resources and reagents should be directed to and will be fulfilled by the Lead Contact, Liang Hong (hong2004@uic.edu).

Materials availability

All plasmids generated in this study will be made available from the lead contact upon reasonable request.

Data and code availability

All data reported in this paper will be shared by the lead contact upon request.

This paper does not report original code.

Any additional information required to reanalyze the data reported in this paper is available from the lead contact upon request.

EXPERIMENTAL MODEL AND SUBJECT DETAILS

Cell culture

HEK293 cells (#85120602, Sigma-Aldrich) were reseeded on coverslips in 6-well plates containing Dulbecco modified Eagle's medium (DMEM, Invitrogen) supplemented with 10% fetal bovine serum (Invitrogen), 100 U/mL penicillin, and 100 μg/mL streptomycin at 37°C under 5% CO_2. After growth to ~70% confluence, cells were transiently transfected with human H_v1 and GFP cDNA plasmids. Recombinant human H_v1 channels were sub-cloned in the pNICE vector. Single-point mutations were introduced with standard PCR techniques. PCR primers were purchased from IDT DNA Technologies. The mutation confirmed by the DNA sequencing was used for subsequent transfection. The HEK-293 cells were transiently transfected with

2 μg of the cDNA encoding H_v1 construct and 0.25 μg of a plasmid encoding enhanced green fluorescent protein (GFP) using Lipofectamine 3000 reagent (Invitrogen; USA) according to the manufacturer's protocol. The mixture was then added to the culture dish and the cells were incubated at 37°C for 24 hours before the electrophysiology studies were conducted. A coverslip with HEK293 cells was placed in a recording chamber containing bath solution on the stage of a fluorescence microscope (Olympus, Japan), and the transfected cells identified by the fluorescent signal emitted from GFP were used for electrophysiological measurements. Patch clamp experiments were conducted 24–48 hours after transfection.

The *Xenopus* oocytes (Stages V and VI) were purchased from Ecocyte Bioscience (USA). Oocytes were kept at 18°C in ND96 medium containing 96 mM NaCl, 2 mM KCl, 1.8 mM CaCl2, 1 mM MgCl2, 10 mM Hepes, 5 mM pyruvate, and 100 μg/mL gentamicin (pH 7.2). The pGEMHE plasmids containing human H_v1 constructs were linearized with NheI restriction enzyme (New England Biolabs, USA). RNA synthesis was carried out with a T7 mMessage mMachine Transcription Kit (Ambion, USA). cRNAs were injected in *Xenopus* oocytes (50 nL/cell, 1.5 μg/μL) 3 days before the electrophysiological measurements.

METHOD DETAILS

Electrophysiological measurements and analysis

H_v1 proton currents in HEK293 cells were measured in whole-cell configuration using an Axopatch 200B amplifier controlled by pClamp11 software through an Axon Digidata 1550B system (all from Molecular Devices, USA). The bath solution contained 75 mM N-methyl-D-glucamine (NMDG), 110 mM 2-(N-morpholino)-ethanesulphonic acid (MES), 80 mM Glucose, 1 mM $MgCl_2$, 1 mM $CaCl_2$, adjusted to pH 6.0 with methanesulfonic acid. The pipette solution contained 75 mM NMDG, 110 mM MES, 80 mM Glucose, 1 mM $MgCl_2$, 1 mM EGTA, adjusted to pH 6.0 with methanesulfonic acid. We used a high H^+ concentration (pH_i = pH_o = 6.0) solution in order to minimize the effects of leak currents mediated by F150 charged mutations on the intracellular H^+ concentration (pH_i), which might generate perturbation on the *G-V* curves. H_v1 proton currents in oocytes were measured in inside-out configuration. Both bath solution and pipette solution contained 100 mM MES, 30 mM tetraethylammonium (TEA) methanesulfonate, 5 mM TEA chloride, 5 mM EGTA, adjusted to pH 6.0 with TEA hydroxide. All measurements were performed at $22 \pm 3°C$. Pipettes had 2-5 MΩ access resistance. Current traces were filtered at 1 kHz and analyzed with Clampfit11 (Molecular Devices) and Origin 2019 (OriginLab).

Steady-state activation *G-V* curves were fitted by the *Boltzmann* equation:

$$G/G_{max} = 1/(1 + \exp(V_{1/2}-V)/k)$$

where G/G_{max} is the relative conductance normalized by the maximal conductance, $V_{1/2}$ is the potential of half activation, *V* is the test pulse, and *k* is the slope factor. *k* is equal to RT/zF, where *z* is the equivalent charge, *R* is the gas constant, *F* is Faraday's constant, and *T* is temperature in *Kelvin*.

Reported $V_{1/2}$ and *k* values derived from the *Boltzmann* fits to data from multiple cells were used to assess the free energy difference at 0 mV (ΔG_0) between the closed and open states of the activation, the ΔG_0 was calculated according to the following:

$$\Delta G_0 = zFV_{1/2}$$

The channel opening time constant T_{act} and closing time constant T_{deact} values were calculated by fitting current traces with the single-exponential equation according to the following:

$$I(t) = I_0 + A(1-\exp(-t/T))$$

where *I(t)* represents the current at time point *t*, I_0 is the initial current amplitude, *T* is the time constant.

Mutant cycle analysis

Double mutant cycle analysis was used to determine whether the effects of two mutations (e.g., mutation 1 at position of F150 in the S2 segment, mutation 2 in the S4 segment) were additive and whether a functional

interaction existed between the two mutation sites. The $|\Delta\Delta G_0|$ (i.e., coupling ΔG_0 value) was determined, and was calculated according to the following:

$$|\Delta\Delta G_0| = | (\Delta G_0^i - \Delta G_0^{WT}) - (\Delta G_0^{ij} - \Delta G_0^j) |$$

where i is the mutation 1, j is the mutation 2. ij is the double mutations at both positions, WT is the wild-type channel.

The standard error of the mean (SEM) value for $|\Delta\Delta G_0|$ was determined, and was calculated according to the following:

$$\text{SEM of } |\Delta\Delta G_0| = \text{SQRT} ((\text{SEM of } \Delta G_0^i)^2 + (\text{SEM of } \Delta G_0^{WT})^2 + (\text{SEM of } \Delta G_0^{ij})^2 + (\text{SEM of } \Delta G_0^j)^2)$$

The large coupling free energy $|\Delta\Delta G_0|$ values indicate functional interactions between positions i and j, and a coupling energy of greater than 4.2 kJ/mol represents a significant interaction between two positions.

QUANTIFICATION AND STATISTICAL ANALYSIS

All data were presented as mean $\pm$ SEM. Significance between means was determined by *Student's* t-test. $p < 0.05$ was considered to indicate a statistically significant difference.